

pubs.acs.org/JPCC Article

Development of Multifunctional Cathode Binder via Inverse Vulcanization for Lithium—Sulfur Battery with Enhanced Capacity Retention

Jisoo Jeong and Thein Kyu*



Cite This: J. Phys. Chem. C 2023, 127, 11836-11844



ACCESS I

III Metrics & More

Article Recommendations

Supporting Information

ABSTRACT: Vinyl-benzaldehyde (VB) monomers containing four functional groups were newly synthesized using the Williamson ether synthesis method. The two aldehyde groups of the synthesized monomers were able to react with amine-terminated macromonomers to form flexible networks. In addition, the two vinyl groups were found to be capable of inverse vulcanization with sulfur by conducting qualitative chemical analysis. The lithium—sulfur battery prepared using the VB-based cathode binder achieved high specific capacity with excellent capacity retention compared to conventional sulfur batteries, demonstrating the potential of the new binder.

Electrode type	Electrode type Before Charge/Discharge	
Conventional sulfur electrode	1 u <u>n</u> .	After 57th cycle
VB vulcanized electrode		After 57 th cycle ^t

1. INTRODUCTION

Growing concerns about fossil fuel depletion and consequential environmental pollution have raised the need for development of rechargeable batteries for long-range, longlife all-electric vehicles. To meet the customers' needs, battery makers and auto industries are developing solid-state batteries for all electric vehicles having high energy densities with good capacity retention.^{2,3} Since a conventional metal oxide-based cathode active material has a limitation of improving battery capacity, various metal complexes have been used to overcome these limitations. The most feasible substance is sulfur, and thus, interest on lithium-sulfur batteries has increased immensely. 4-6 There are several advantages of using sulfur as a cathode material since it is abundantly available on earth and relatively cheap, i.e., about 20% of the price of nickel manganese cobalt oxide cathode active materials. Moreover, sulfur is made up of eight elements forming a ring with a theoretical specific capacity value of 1672 mA h g⁻¹, which is significantly higher than that of lithium iron phosphate (i.e., 170 mA h g⁻¹). However, there are some disadvantages in infusing sulfur directly into the cathode because its electrical and/or ionic conductivities are inherently poor. Especially, excessive volume expansion or contraction can occur in the sulfur cathode during charging/discharging, which is detriment to the battery life, accompanied by poor charge retention, resulting in premature battery failure.8 In addition, the asprepared sulfur-carbon cathode does not have lithium ions initially and thus the lithium metal anode has been customarily used as a lithium ion source to continuously supply Li ions to the sulfur-carbon electrode through a so-called "pre-lithiation" process.

In a lithium-sulfur battery, lithium and elemental sulfur can form various polysulfide derivatives following reduction reaction during the discharging cycle.⁵ The higher order polysulfide that is transported to the anode reduces the amount of active materials in the cathode, thereby compromising the battery performance caused by the formation of solid electrolyte interface layer at the anode and resulting in a decrease in specific capacity. 10 To alleviate such problems, various chemical and physical inhibition methods have been actively pursued by encapsulating the periphery of sulfur with carbon or inserting sulfur in porous carbon and/or in carbon nanotubes. 11,12 There are several methods for chemically preventing the shuttling effect of the polysulfide derivatives, such as making a chemical anchor or trapping lithium sulfide in the form of nanometal oxide. 13,14 A typical chemical inhibition method is inverse vulcanization, i.e., crosslinking sulfur chains with macromonomer precursors containing carbon-carbon double bonds. 15 The reason as to why the capacity retention is improved by using the inverse vulcanization method is that the amount of sulfur loss can be minimized via linking the loworder polysulfide derivatives to the polymeric network. 16,17 Another approach is to use the sulfur-containing monomer. To eliminate the polysulfide dissolution, recent studies on applying C-S bonds, using short sulfur units in sulfurized

 Received:
 March 29, 2023

 Revised:
 May 31, 2023

 Published:
 June 15, 2023





polyacrylonitrile (SPAN) or organo-sulfur, have been extensively explored. $^{18-20}$

Recently, vinyl-benzaldehyde (VB) monomer has been employed as a coupling agent to form the covalent organic framework, which in turn can improve thermal and chemical stability with potential applications in lithium—sulfur batteries. Alternatively, star-shaped macromolecules may be synthesized through RAFT polymerization using the VB monomer. ²³

In the present article, a new type of VB monomer was designed and synthesized to develop cathode active material, in which the two aldehyde groups could react with multi-armed amine groups²⁴ to form a flexible polymeric network, while the other two vinyl groups further react with the sulfur chains via a so-called "inverse-vulcanization". Subsequently, the electrochemical performance of the inverse vulcanized sulfur cathode is evaluated and compared with those of a conventional lithium—sulfur battery. Research on improvement of ion mobility has been actively conducted over the past few decades. The VB-sulfur inverse vulcanized cathode or the cathode containing conventional sulfur was prepared, and their electrochemical stability was investigated with dimethoxyethane (DME)/dioxolane (DOL) solvent (1/1 ratio by volume) in combination with thin gel polyelectrolyte (GPE) membrane containing LiTFSI salt.

2. EXPERIMENTAL SECTION

- **2.1. Materials.** To synthesize the VB monomer, 3-allylsalicylaldehyde, 1,2-dibromoethane, potassium carbonate (K_2CO_3), dimethylformamide (DMF), sodium sulfate (Na_2SO_4), and ethyl acetate (EA) were purchased from Sigma-Aldrich and used as received. For the GPE polymer precursor materials, trimethylolpropane ethoxylate triacrylate (TMPETA), 2,2-dimethoxy-2-phenylacetophenone (DMPA), 1,3-dioxolane(DOL), and 1,2-dimethoxyethane(DME) were obtained from Sigma-Aldrich, whereas lithium bis-(trifluoromethane sulfonyl)imide (LiTFSI) was purchased from Solvay. For the electrode materials, sulfur, poly-(vinylidene fluoride) (PVDF, Mw of 534,000), and N-methyl-2-pyrrolidone (NMP) were acquired from Sigma-Aldrich. Lithium chip (600 μ m) was purchased from MSE supplies. MWCNT was kindly provided by LG Chem.
- 2.2. Synthesis of 2,2'-(Ethane-1,2-diylbis(oxy))bis(3allylbenzaldehyde). In order to synthesize the new VB monomer, the Williamson ether synthesis method was adopted to introduce the ether linkage reaction. 1 g (6.1 mmol) of 3allylsalicylaldehyde was poured into a flask with 20 mL of DMF and stirred under nitrogen for 30 min. Subsequently, 0.84 g (6.1 mmol) of K₂CO₃ was added and stirred for another 2 h, and then 0.57 g (3.05 mmol) of 2-dibromoethane was added dropwise using a funnel at a constant rate for 1 h and heated to 90 °C to allow the reaction in a nitrogen environment for additional 10 h. Upon completion of the reaction, DMF solvent was evaporated using a rotary evaporator, and the remaining chemical was extracted by washing with EA and DI water. After collecting the organic layer substrate, Na₂SO₄ was added and stirred to remove the moisture and then filtered. The organic substrate was further dried in a vacuum oven at 45 °C for 24 h, and the transparent yellow powders were obtained; the yield of VB was 67%.
- **2.3. Inverse Vulcanization.** 3 g of sulfur was melted in a beaker at 185 °C to ensure the breakage of the octagonal sulfur ring. Subsequently, 1 g of VB monomer was added and stirred

- for 10 min. After cooling, the solution became a hard brown solid at room temperature, which was transferred into EA and stirred for 12 h and then filtered to remove unreacted VB monomer. After drying in a vacuum oven at 45 °C for 12 h, the conversion was over 90%. Fine powders were obtained by ball milling for use as a cathode active material.
- 2.4. Preparation of Cathode Slurry. The slurry containing 80 wt % of the inverse vulcanized sulfur cathode was prepared by mixing with 10 wt % of PVDF and 10 wt % of MWCNT uniformly dispersed in NMP. At this stage, the viscosity of the resin slurry was between 5000 and 10,000 c-Poise. This slurry was spread uniformly on aluminum foil using a film applicator. Thereafter, it was dried in a vacuum oven at 120 °C for 24 h. After calendering by cross-rolling, the final thickness was $50 \pm 2 \mu m$. For the purpose of comparison, another cathode slurry containing 80 wt % of regular sulfur powder, 10 wt % of PVDF, and 10 wt % of MWCNT slurry was prepared in accordance with the same procedures mentioned above. At this time, the loading amount of elemental sulfur in the inverse vulcanized cathode and conventional sulfur cathode were 2.0² and 2.4 mg cm⁻², respectively.
- **2.5.** Preparation of Gel Polymer Electrolytes. DME and DOL were mixed in a volume ratio of 1:1 together with 1 M LiTFSI under the argon gas environment. Subsequently, TMPETA containing 3 wt % of a DMPA photo-initiator was added to the dissolved salt solution in the ratio of 20/80 wt % of TMPETA polymer precursor/LiTFSI dissolved in DME/DOL and stirred for 12 h. The precursor solution was a colorless, transparent viscous liquid. Thereafter, the precursor melt mixture was poured directly onto the CNT-sulfur cathode, which was already coated on the aluminum foil, and then uniformly spread using a film applicator. Photopolymerization was performed immediately by subjecting them to uniform exposure to UV light at a wavelength of 365 nm and an intensity of 10 W cm⁻² for 30 s. The thickness of the GPE was about 30 μ m with 15 mL g⁻¹ of the fixed electrolyte/sulfur ratio.
- **2.6. Fabrication of Batteries.** The specimen coated with the cathode and GPE on the aluminum foil was cut to the area of $1.0~{\rm cm}^2$. In order to assemble a battery, the aforementioned electrode was moved to a glove box in an argon gas environment. CR2032 coin cell batteries for the cyclic voltammetry (CV) and charge/discharge cycler were prepared using Li metal precut chip (600 μ m thick) as electrode. The linear sweep voltammetry (LSV) test was performed in the lithium metal/GPE/stainless steel electrode configuration.
- **2.7. Measurements.** In order to measure the melting temperature $(T_{\rm m})$ of the synthesized monomer, the amount of 5 mg of a sample was collected from each sample, placed in a DSC aluminum pan, and crimped it by encapsulation machine. The sample was cooled to $-50~^{\circ}{\rm C}$ from room temperature with a reference pan using DSC (Q200, TA instrument) and then held under the isothermal condition for 10 min. The DSC was performed with a constant ramping rate of $10~^{\circ}{\rm C}$ min $^{-1}$ to $200~^{\circ}{\rm C}$. $^{1}{\rm H}$ NMR spectra were acquired by means of a Varian 500 MHz spectroscopy using deuterated chloroform as the solvent. To analyze the VB-sulfur vulcanized crosslinked material, Fourier transform infrared (FTIR) spectral analysis was conducted using a Nicolet 6700 FTIR Spectrometer (Thermo) with 32 scans at a resolution of 4 cm $^{-1}$ within the range of $400-4000~{\rm cm}^{-1}$.

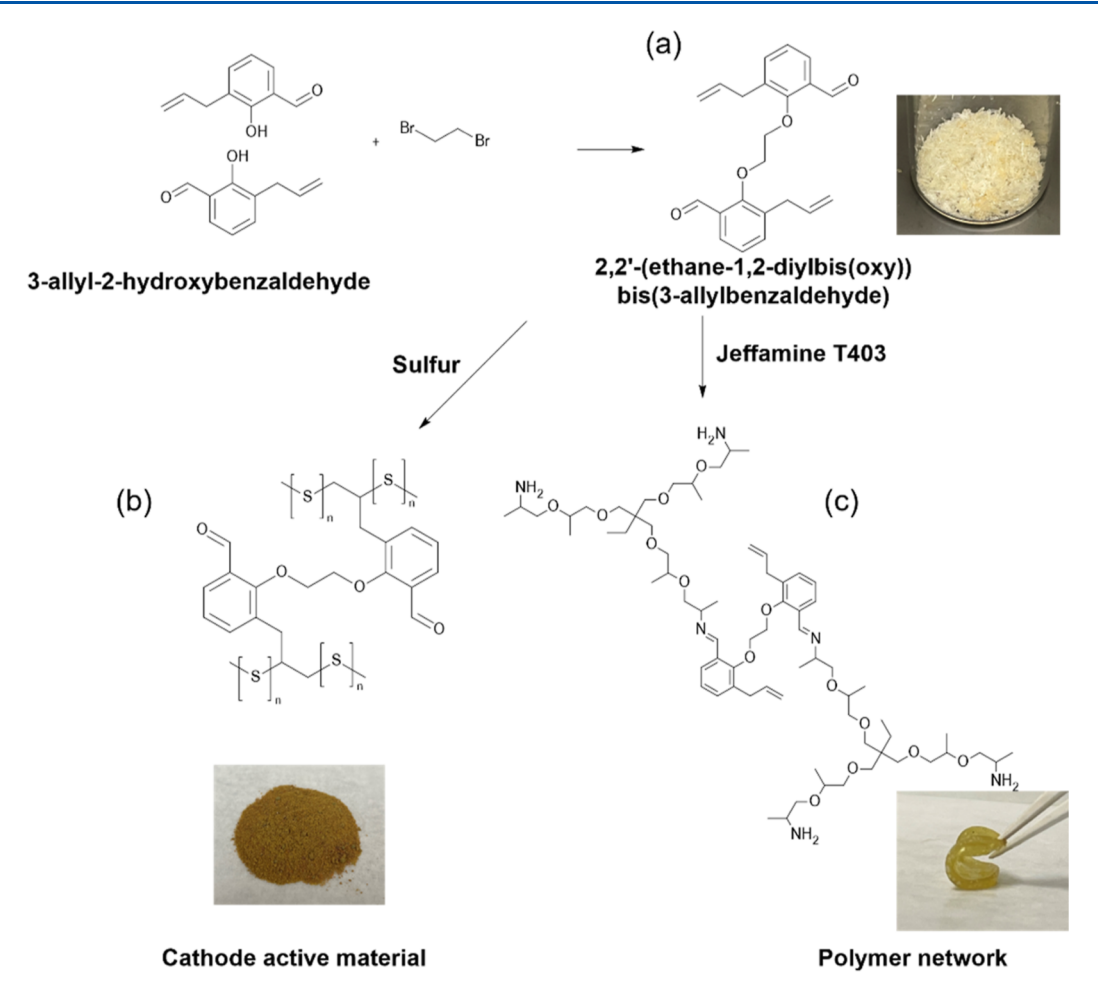


Figure 1. (a) Synthesis of VB monomer and (b) its inverse vulcanization for cathode active material along with their respective photographs in powder forms (c) elastomer obtained via Schiff reaction with amine terminated Jeffamine T403.

The batteries containing sulfur cathode combined with GPE were subjected to CV at room temperature using potentiostats (Autolab, Mettom) to evaluate their electrochemical performance. Charge/discharge cycling was performed over the potential range of a lithium—sulfur battery at different C rates using an MTI 8-channel battery analyzer at room temperature.

3. RESULTS AND DISCUSSION

First, VB monomers with two bonds and two aldehyde groups and an ether linkage in the middle of the chain were first synthesized following the Williamson ether synthesis scheme^{27–29} of 3-alylsalicylaldehyde using 1,2-dibromoethane, as depicted in Figure 1. For the application to lithium-sulfur batteries, the double bonds of the synthesized VB monomer were induced to undergo radical polymerization with sulfur, as illustrated in Figure 1b, so that it could be used as the cathode active material in lithium-sulfur batteries via inverse vulcanization. In addition, as shown in Figure 1c, the two aldehyde groups have the ability to form imine groups by dehydration and condensation reactions with amine groups to create another polymer network, thus allowing for the preparation of covalent organic network, as described in the Supporting Information. Upon synthesizing the VB monomer, the yield of the reaction was 67%. Figure S1a shows the NMR spectrum of 3-allylsalicylaldehyde, one of the chemicals used to synthesize the VB monomer. In the NMR analysis, hydrogens that are

dependent on the benzene structure appear between 6 and 7.5 ppm. A single hydrogen attached to the carbon of the aldehyde group appeared as a singlet at 9.9 ppm and the hydroxyl group also appeared as a singlet at 11.3 ppm. The hydrogens in the allyl group with double bonds appeared clearly below 5.1 ppm. Figure S1b shows the NMR characterization of the VB monomer synthesized by the reaction of two 3-allylsalicylaldehydes with dibromo benzene. A new peak of ethylene group from dibromo benzene appeared at 4.3 ppm. The hydroxyl group bound to 3-Allylsalicylaldehyde was converted into a hetero-linkage upon reaction with dibromo benzene, causing the hydrogen peak at 11.3 ppm to disappear. Other characteristic peaks were slightly shifted but did not deviate significantly from their original positions.

Furthermore, as shown in Figure 2a, the FTIR spectrum of the synthesized VB monomer no longer reveals the hydroxyl peak of 3-allylsalicylaldehyde between 3000 and 4000 cm⁻¹, indicating that the unreacted monomer was neatly removed, leaving only the VB monomer that had completely reacted with 1,2-dibromoethane. The vinyl group, which can react with sulfur, was present at 5.1 ppm in the NMR spectrum. The aldehyde group was located at 10 ppm in the NMR spectrum, while a characteristic peak was found at 1677 cm⁻¹ in the IR spectrum. To prepare the inverse vulcanized cathode active material for lithium—sulfur batteries, the obtained VB was reacted with sulfur and subjected to infrared spectroscopy qualitative analysis. The peak of sulfur appeared in the 3500

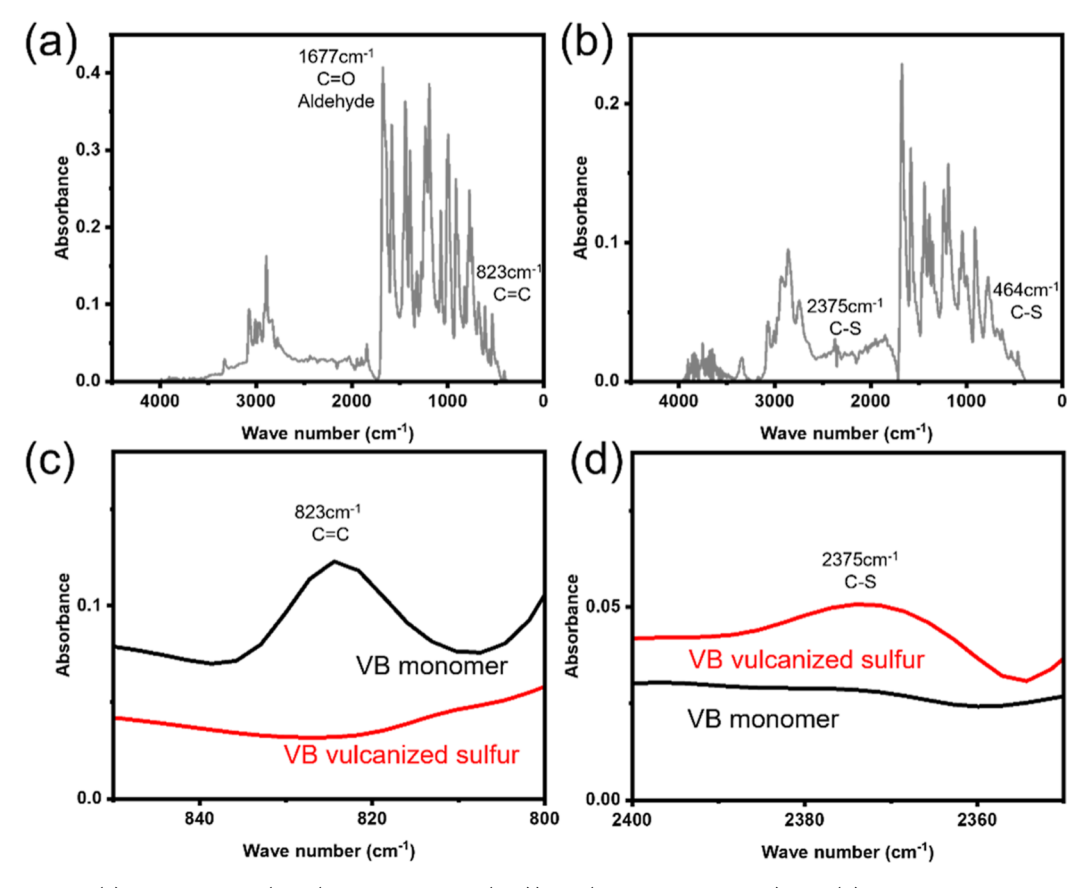


Figure 2. IR spectra of (a) VB monomer (2,2'-(ethane-1,2-diylbis(oxy)) bis (3-allylbenzaldehyde) and (b) VB monomer after vulcanization with sulfur (c) showing the depletion of C=C twisting from VB and (d) emergence of C-S peak indicative of the vulcanization reaction.

cm⁻¹ band, and carbon-sulfur bonds exhibited characteristic peak³⁰ at 475 and 2375 cm⁻¹ (Figure 2b). The VB-sulfur crosslinked material exhibits a distinct peak at 823 cm⁻¹ corresponding to the C=C twisting of vinyl group, implying nearly complete consumption of the C=C double bonds (Figure 2c,d) with the degree of conversion is over 90%.

To investigate the electrochemical performance of the cathode active materials prepared from VB monomer, the CR2032 type of lithium—sulfur battery cell was assembled. The electrodes containing the VB-sulfur crosslinked material contained about 3 mg cm $^{-2}$ of the effective sulfur, and the high ionic conductive GPE (Figure S2a) was prepared by mixing a polyethylene glycol-type precursor with 1 M of LiTFSI dissolved in a 1,2-dimethoxyethane (DME)/1,3-dioxolane (DOL) (50/50) solvent and then photo-crosslinking to form a gel network between the lithium metal anode and the inverse vulcanized sulfur cathode. The 25 μ m thickness of GPE was prepared by adding 45 μ L of liquid electrolyte and adjusting the weight ratio of the liquid electrolyte to the cathode active material, i.e., sulfur to be 15 μ L mg $^{-1}$.

CV tests were performed on assembled between the lithium metal anode and VB-sulfur cathode of the battery cell. In the CV curve, the reduction and oxidation peaks of the inverse vulcanized sulfur cathode were observed between 1.5 and 3 V (Figure 3). At a scanning rate of 0.1 mV s⁻¹, a single oxidation peak occurring at the cathode can be discerned at 2.6 V during the battery charging cycle, whereas two reduction peaks appeared at about 1.8 and 2.2 V during battery discharging. Moreover, the five scans acquired at 0.1 mV s⁻¹ scan rate were virtually overlapped suggestive of the fact that the redox

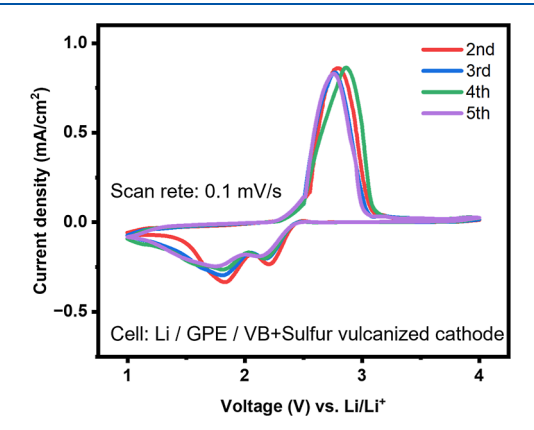


Figure 3. CV of a battery assembled with DME/DOL plasticized GPE with the VB-sulfur vulcanized cathode showing dual reduction peaks at a scanning rate of 0.1 mV $\rm s^{-1}.$

reaction of the inverse vulcanized VB-sulfur system was indeed reproducible and reversible. 31,32

Next, the effect of inverse vulcanization on the sulfur cathode on the electrochemical performance is demonstrated in Figure 4a,b. The conventional sulfur cathode of the tested battery was composed of a combination of elemental sulfur powder without any treatment and PVDF binder and carbon-based conductor for electron conduction. The prepared two cathodes were subjected to galvanostatic charging and discharging tests based on a lithium metal anode battery at a voltage range of 1.7 to 2.6 V, which corresponded to the oxidation and reduction potentials obtained from the CV

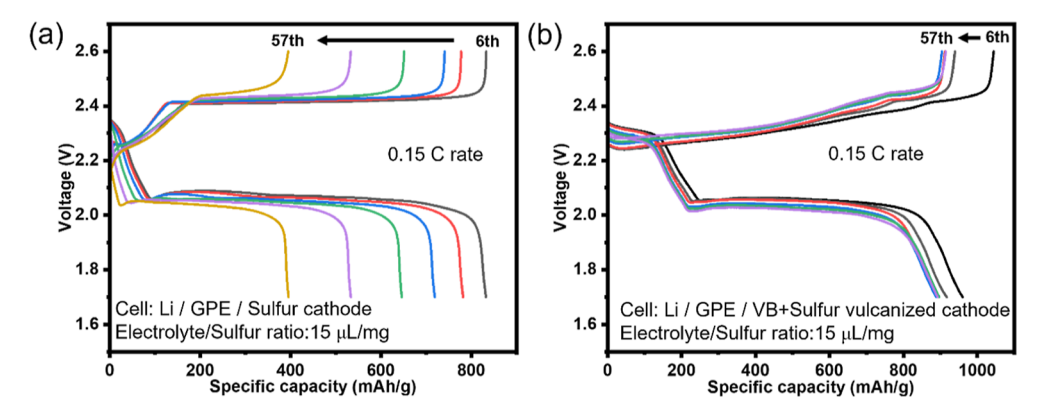


Figure 4. Comparison of cyclic performances of lithium—sulfur batteries in various Li/GPE/sulfur cathode configurations: cyclic performance of inverse vulcanized lithium—sulfur battery. (a) Cyclic performance of the referenced sulfur cathode battery at a 0.15 C rate showing rapid capacity decay and (b) cyclic performance of inverse vulcanized lithium—sulfur cathode battery rate showing enhanced specific capacity with stable capacity retention at 0.15 C.

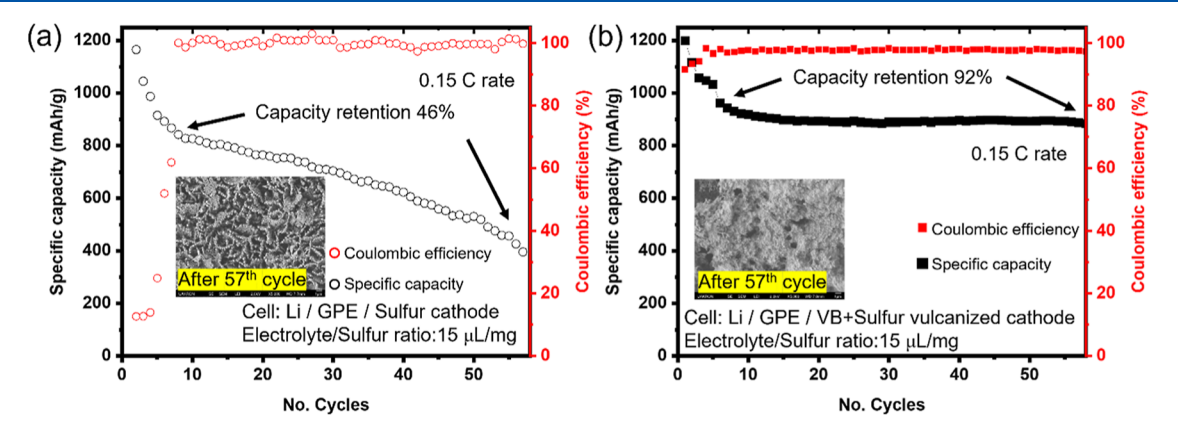


Figure 5. Comparison of specific capacity and Coulombic efficiency of a battery (a) using neat sulfur electrodes and a battery (b) using VB-sulfur vulcanized electrodes. The charge/discharge cycle evaluation was performed at the same rate of 0.15 C for both batteries. The corresponding zoomed-in SEM micrographs after 57th cycles, showing (a—inset) phase separated structure suggestive of failed battery and (b—inset) smooth surface morphology after 57th cycles, indicative of stable character.

shown in Figure 3. The battery with the VB-sulfur vulcanized cathode was subjected to a constant current condition of 0.45 mA cm⁻², while the battery with the reference sulfur cathode was subjected to a current of 0.48 mA cm⁻² as it contained 3.2 mg of cathode active material. By comparing the charge and discharge profiles from the 6th cycle to the 57th cycle shown in Figure 4a, the initial capacity stabilized at a certain level of the elemental sulfur in the cathode showed a sharp decrease in the specific capacity as the number of cycles increased. In other words, during the discharge process, sulfur was reduced to polysulfide by combining with lithium ions, and the long-chain polysulfide was dissolved in the liquid electrolyte, causing a shuttle effect. It may be conjectured that the cathode active material, i.e., sulfur, departed from the cathode. 33-35 Notably, compared to the conventional sulfur cathode, the VB monomer with inverse vulcanized sulfur not only showed a higher capacity of the cathode active material, but the capacity decayed very slowly with repeated cycles (Figure 4b). Moreover, the dual voltage plateaus in discharge (reduction) cycles virtually overlapped and persisted for all 50 cycles thus tested, suggestive of improved charge retention. The observed dual plateaus are typical features of conventional lithiumsulfur battery, which are often attributed to the progressive conversion of higher order solid elemental sulfur to lower order soluble polysulfide derivatives during cycling.³⁶ In addition, the difference between the voltages at which

oxidation and reduction are triggered gradually widens as cycles are repeated. While the conventional sulfur battery showed a difference of more than 0.2 V, the battery with the VB monomer applied to the sulfur exhibited a difference of only about 0.1 V, indicating that the improved charge and discharge performance, which may be attributed to the excellent compatibility of VB and sulfur.

Figure 5 illustrates the change in specific capacity and the Coulombic efficiency over the cycle for a battery using conventional sulfur and a battery using inverse vulcanized sulfur and VB. Both batteries had an initial specific capacity of about 1200 mA h g⁻¹ for the first few cycles, which corresponds to the battery conditioning process, which then stabilized at about 950 and 840 mA h g⁻¹. With the conventional sulfur electrode, capacity decay occurred rapidly as charge and discharge cycles continued, resulting in a capacity retention of approximately 46% after 50 cycles (Figure 5a). This rapid decay can be explained by the lack of physical and chemical barriers to prevent the migration of polysulfide in conventional sulfur electrodes, resulting in a shuttling effect that reduces the amount of cathode active material. The Coulombic efficiency of both batteries exhibited high efficiency after initial stabilization, but the charge/discharge efficiency fluctuation exhibited greater variation for the conventional sulfur electrode battery due to the noticeable decline in specific capacity with each cycle.

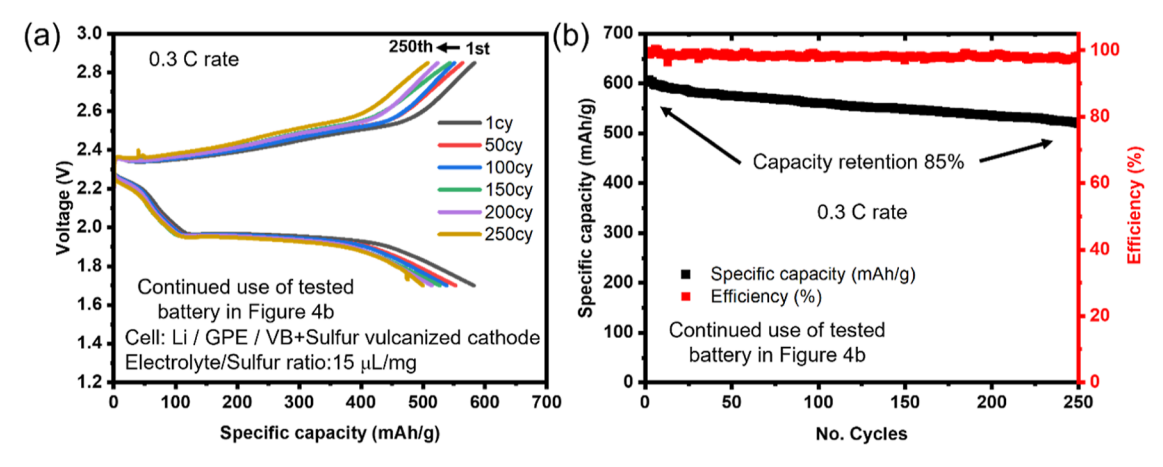


Figure 6. Evaluation of charge and discharge performance of a battery with VB-sulfur vulcanized electrodes, which had already been previously evaluated for 57 cycles at a 0.15 C rate in Figure 4b, to determine long-term stability at higher C rate (0.3 C rate). (a) Charge/discharge profile over 250 cycles (b) Discharge capacity and Coulombic efficiency as a function of cycles.

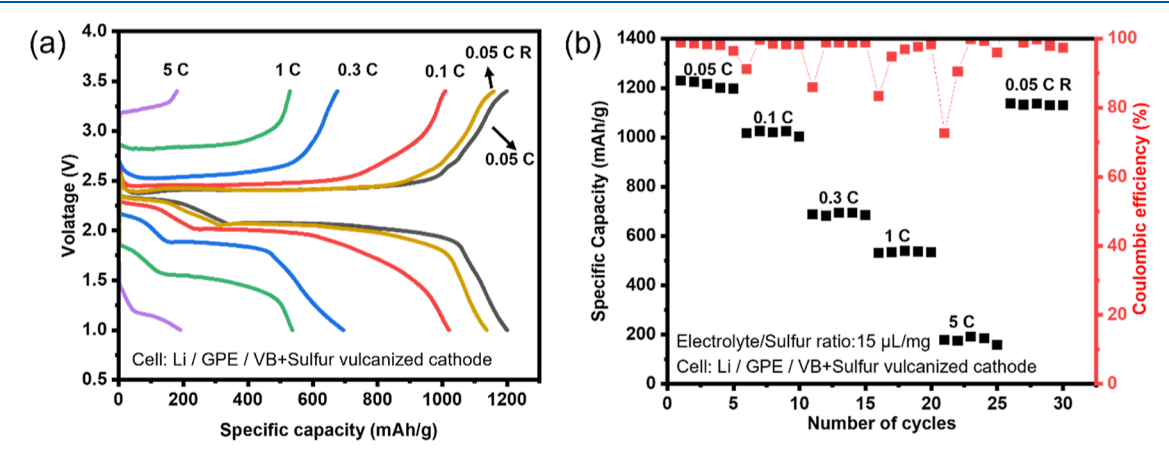


Figure 7. Charge/discharge behavior of lithium—sulfur battery in Li metal anode/GPE/VB-sulfur vulcanized cathode battery configuration; (a) charge/discharge curves showing the variation of voltage as a function of various C rates and (b) specific capacity and Coulombic efficiency as a result of variation in C rate.

On the other hand, as shown in Figure 5b, the inverse vulcanized VB-sulfur cathode revealed a capacity retention rate of about 92% with less decrease in capacity over repeated cycles. The inverse vulcanized VB-sulfur cathode, sulfur attached to a C=C double-bond of the VB matrix can undergo complexation with lithium ions, which suppresses the polysulfide shuttle effect. Hence, lithium ions can travel back and forth from cathode to anode readily, so the capacity retention can be expected to improve (Figure 4b). 16,37 It should be pointed out that the specific capacity data presented here are calculated based on charge per unit mass of sulfur, the actual loading of sulfur on a given electrode should be based on the fraction of sulfur in the cathode material. Moreover, the aldehyde groups in the ether-linked benzaldehyde residue can effectively dilute (or reduce) the sulfur content and thus the actual capacity value could be higher.

The SEM images in the insets of Figure 5a,b show the surface morphology of the sulfur cathode of standard sulfur cathode and VB-inverse vulcanized cathode after 12 h of immersion in DME/DOL electrolyte. Note that batteries based on conventional sulfur electrodes and VB-sulfur electrodes were subjected to 57 cycles of charge/discharge testing and then stopped during the discharge process to check for lithium sulfide elution. The batteries were then disassembled, and the electrodes were immersed in liquid DME/DOL electrolyte.

The observed phase separated morphology suggests that most of the unreacted active materials on the conventional sulfur electrode have disappeared (or unreacted sulfur was extracted by dissolving in DME/DOL solvent), leaving only the PVDF and conductive carbon material. In contrast, the VB-sulfur electrode showed a smooth electrode surface with only limited of the active material, if any, disappearing after 57 cycles. This indicates that the sulfur in the VB—vulcanized cathode is no longer soluble in DME/DOL liquid electrolyte, thereby retaining the smooth surface morphology. Consequently, the shuttle effect can be suppressed sufficiently leading to the stable capacity retention, which may be ascribed to the effect of VB inverse vulcanization of the lithium sulfur cathode.

Of particular interest is that the VB-sulfur vulcanized battery used in Figure 4b was still active; therefore, it was evaluated in succession for an additional 250 cycles at a faster rate of 0.3 C rate to determine cyclic stability. Figure 6a shows the charging and discharging profiles acquired every 50 cycles. The voltage was scanned between 1.7 and 2.85 V to cycle the charge and discharge processes with the current density of about 0.9 mA cm⁻². The discharge curve revealed two distinct plateaus in which the charge and discharge profile curves virtually overlapped until 250 cycles, indicating that there is no significant degradation of the VB-sulfur vulcanized cathode active material due to the change in the applied C rate from

0.15 to 0.3 C. However, at 0.15 C in Figure 4b, the starting potentials of charge and discharge were not much different at 2.3 V. However, as the charging and discharging evaluation rate increased, the charging starting voltage was close to 2.4 V and the discharging voltage was 2.25 V, indicating a slight difference in oxidation and reduction potentials as the C rate increased.

Figure 6b shows a diagram showing the specific capacity and the Coulombic efficiency of the same battery at 0.3 C rate. The Coulombic efficiency (indicating the energy storage and release efficiency) of the battery based on the VB-sulfur vulcanized electrode was maintained at about 98% for hundreds of cycles even at a faster rate of 0.3 C rate, proving the excellent retention efficiency of VB-sulfur inverse vulcanized lithium—sulfur battery with high specific capacity. Since the battery cycling experiment was conducted after testing at 0.15 C, no discernible capacity drop was noticed. Following the initial 57 cycles at 0.15 C test, the starting specific capacity at 0.3 C rate was about 600 mA h g⁻¹. After subsequent 250 cycles, the capacity still remained at 85% without any significant drop.

Lithium—sulfur batteries need to be tested at a variety of C rates, as their capacity and energy density can vary greatly depending on the rate of charge and discharge. Charging and discharging at a high C rate provides the advantage of quickly storing energy, though it also generates more heat inside the battery, which can reduce the battery's performance, whereas charging and discharging at a low C rate can store a high amount of energy but requires a longer time. Therefore, the charging and discharging tests of lithium—sulfur batteries with VB-sulfur vulcanized electrodes at various rates were conducted to derive the specific capacity, operating voltage, and internal resistance, as shown in Figure 7, to explore the optimal battery characteristics.

As shown in Figure 7a, charging and discharging at 0.05 C rate resulted in the highest specific capacity of about 1200 mA h g^{-1} . This implies that as the C rate is gradually decreased, i.e., charging is performed at a slower rate, the specific capacity improves, and the theoretical specific capacity of 1675 mA h g⁻¹ may be achieved by charging at an extremely slow rate. On the contrary, as the C rate gradually increases, the specific capacity gradually decreases, with a specific capacity value of about 685 mA h g⁻¹ at 0.3 C. The reason for a slightly higher capacity value relative to that (600 mA h g⁻¹) in Figure 6 is due to the self-recovery of the battery during rest following the test at 0.15 C for initial 57 cycles. Of particular importance is the fact that as the charge and discharge rate gradually increased, the starting voltage of the discharge of the lithiumsulfur battery gradually decreased from 2.4 to 1.5 V, and the charging voltage gradually increased from 2.2 to 3.2 V.⁴³ What this means is that the internal resistance of the battery increased, resulting in a gradual increase in the difference between the starting voltage of charge and discharge. Figure 7b presents the measured specific capacity and the Coulombic efficiency as the charge and discharge tests were performed by starting at 0.05 C and changing to various C rates up to 5 C, and then reverting the charge and discharge tests back to 0.05 C. The results show a systematic decrease in the specific capacity value of the battery as the charge and discharge rate increased. In particular, when returned to 0.05 C, the charge/ discharge curve recovered close to its original position at 0.05 C, demonstrating the stable nature of the charge/discharge cycling behavior of the battery with VB-sulfur inverse

vulcanized electrode. It should be pointed out that there is a sudden drop in the Columbic efficiency in each step of changing C rate. This observation may be due to fact that only the materials at the electrode interface will be active initially, and thus there may be some amount of sulfur in the bulk which may not be accessible immediately. As a consequence, there is slight delay in catching up in the Coulombic efficiency as manifested in the sudden drop in Figure 7b.

As can be seen in Figure 7a, the variation of the discharge voltage plateau with C rate shows the fairly consistent specific capacity trends of VB-sulfur battery. The C rate-dependent specific capacity is tabulated in Table 1 along with the

Table 1. Energy Density and Power Density of VB-Sulfur Electrode at Various C Rates

C rate (1/h)	VB-sulfur cathode Specific capacity (mA h/g)	voltage Plateau (V)	energy density (W h/Kg)	Power density (W/Kg)
0.05	1201	2.3, 2.1	2762	138
0.1	1002	2.2, 2.0	2255	225
0.3	685	2.1, 1.8	1439	432
1	533	1.8, 1.5	959	959
5	158	1.5, 1.1	237	1185

corresponding reduction voltage plateau, energy density, and power density. As the C rate decreases, the discharge time gets longer, which gives more time for the charge transport to complete. Consequently, the specific capacity and operating voltage gradually improve. This indicates that the energy density increases with increasing C rate, while the power density, which is the parameter of energy density divided by time, decreases. Therefore, the charge/discharge rate at which the energy density and power density exhibit optimal performance could be between 0.3 and 1 C, although this may vary depending on the application requiring high power output or sustained energy storage system. 44,45 With this potential performance, the new VB monomer can be expected to be suitable as a cathode active material for high power, high energy lithium-sulfur batteries via inverse vulcanization reaction of VB with sulfur cathode.

4. CONCLUSIONS

In summary, a new monomer of VB type with two carbon-carbon double bonds and two aldehyde groups was synthesized. Using the Williamson ether synthesis reaction, 3-allylsalicylaldehyde and 1,2-dibromoethane were synthesized in a one-step reaction, and the product (VB) was further characterized by ¹H NMR and FT-IR analysis. The two aldehyde groups of the newly synthesized VB monomer could be copolymerized with amine-based monomers to form polymer networks, and the two carbon—carbon double bonds could undergo radical polymerization. In particular, in this study, the two carbon—carbon double bonds were reacted with sulfur through inverse vulcanization and applied to lithium—sulfur batteries, a next-generation battery.

What is notably interesting is that when this cathode is combined with DME/DOL plasticized GPE in lithium metal batteries, the redox characteristic peak of sulfur between 1.5 and 2.5 V in CV tests is continuously reproducible and highly stable. In the charge/discharge test, a high specific capacity value of about 950 mA h g⁻¹ was obtained at 0.15 C, with an excellent Coulombic efficiency of over 98% for 50 cycles,

giving a superior capacity retention of about 92%. Long-term charge/discharge cycle testing at 0.3 C for an additional 250 cycles also demonstrated a capacity retention of 85%. On the other hand, for the conventional sulfur cathode, the specific capacity decreased significantly from 840 to 390 mA h g⁻¹ as the number of cycles increased, demonstrating that inverse vulcanization of the sulfur cathode with VB plays an important role in improving the specific capacity and maintaining superior capacity compared to the conventional sulfur cathode. It can be concluded that the electrochemical performance of lithium-sulfur batteries strongly depends on the VB vulcanized sulfur cathode utilized in this way, and the VB monomer can point out the important role of inverse vulcanization in lithium-sulfur batteries for high specific capacity and good capacity retention over 300 cycles. Therefore, VB monomers can be expected to have applications in preventing the rapid capacity degradation of conventional lithium-sulfur batteries and have the potential for selective chemical reactions with various functional groups.

ASSOCIATED CONTENT

5 Supporting Information

The Supporting Information is available free of charge at https://pubs.acs.org/doi/10.1021/acs.jpcc.3c02096.

H NMR spectra, FT-IR spectrum and DSC thermal analysis of the VB monomer, ionic conductivity, and LSV plots of the GPE used in the battery and additional CV graphs as a function of scan rate for the VB-sulfur cathode (PDF)

AUTHOR INFORMATION

Corresponding Author

Thein Kyu — School of Polymer Science and Polymer Engineering, University of Akron, Akron, Ohio 44325, United States; orcid.org/0000-0002-6302-0784; Email: tkyu@uakron.edu

Author

Jisoo Jeong — School of Polymer Science and Polymer Engineering, University of Akron, Akron, Ohio 44325, United States; ⊚ orcid.org/0009-0004-7809-4884

Complete contact information is available at: https://pubs.acs.org/10.1021/acs.jpcc.3c02096

Notes

The authors declare no competing financial interest.

ACKNOWLEDGMENTS

This work was supported by the National Science Foundation under grant no. PFI-2214006.

REFERENCES

- (1) Yang, C. Running battery electric vehicles with extended range: Coupling cost and energy analysis. *Appl. Energy* **2022**, *306*, 118116.
- (2) Sevilla, A. R.; Gao, H.; Steinberg, K. J.; Gallant, B. M. Elucidating Concentration-Dependent Energy Limitations in Li Primary Battery Fluoro-organosulfur Catholytes. *J. Phys. Chem. C* **2023**, *127*, 1722–1732.
- (3) Kimura, T.; Nakano, T.; Sakuda, A.; Tatsumisago, M.; Hayashi, A. Hydration and Dehydration Behavior of Li4SnS4 for Applications as a Moisture-Resistant All-Solid-State Battery Electrolyte. *J. Phys. Chem. C* 2023, *127*, 1303–1309.

- (4) Shin, H.; Baek, M.; Gupta, A.; Char, K.; Manthiram, A.; Choi, J. W. Recent progress in high donor electrolytes for lithium—sulfur batteries. *Adv. Energy Mater.* **2020**, *10*, 2001456.
- (5) Fang, R.; Zhao, S.; Sun, Z.; Wang, D. W.; Cheng, H. M.; Li, F. More reliable lithium-sulfur batteries: status, solutions and prospects. *Adv. Mater.* **2017**, *29*, 1606823.
- (6) Liu, J.; Cao, Y.; Zhou, J.; Wang, M.; Chen, H.; Yang, T.; Sun, Y.; Qian, T.; Yan, C. Artificial lithium isopropyl-sulfide macromolecules as an ion-selective interface for long-life lithium—sulfur batteries. *ACS Appl. Mater. Interfaces* **2020**, *12*, 54537—54544.
- (7) Gupta, V.; Germida, J. J. Microbial transformations of sulfur in soil. In *Principles and Applications of Soil Microbiology*; Elsevier, 2021; pp 489–522.
- (8) Yan, C.; Zhou, Y.; Cheng, H.; Orenstein, R.; Zhu, P.; Yildiz, O.; Bradford, P.; Jur, J.; Wu, N.; Dirican, M.; et al. Interconnected cathode-electrolyte double-layer enabling continuous Li-ion conduction throughout solid-state Li-S battery. *Energy Storage* **2022**, *44*, 136–144.
- (9) Wang, G.; Li, F.; Liu, D.; Zheng, D.; Abeggien, C. J.; Luo, Y.; Yang, X.-Q.; Ding, T.; Qu, D. High performance lithium-ion and lithium-sulfur batteries using prelithiated phosphorus/carbon composite anode. *Energy Storage* **2020**, *24*, 147–152.
- (10) Cheng, Q.; Xu, W.; Qin, S.; Das, S.; Jin, T.; Li, A.; Li, A. C.; Qie, B.; Yao, P.; Zhai, H.; et al. Full dissolution of the whole lithium sulfide family (Li2S8 to Li2S) in a safe eutectic solvent for rechargeable lithium—sulfur batteries. *Angew. Chem.* **2019**, *131*, 5613—5617.
- (11) Gohari, S.; Yaftian, M. R.; Sovizi, M. R.; Tokur, M.; Shayani-Jam, H.; Sharafi, H. R. A parametric study on encapsulation of elemental sulfur inside CNTs by sonically assisted capillary method: Cathodic material for rechargeable Li–S batteries. *Microporous Mesoporous Mater.* **2022**, *340*, 112033.
- (12) Li, R.; Dai, Y.; Zhu, W.; Xiao, M.; Dong, Z.; Yu, Z.; Xiao, H.; Yang, T. Construction of porous carbon nanofibers with encapsulated sulfur as free-standing cathode material of lithium-sulfur batteries. *Ionics* **2022**, *28*, 2155–2162.
- (13) Sun, Z.; Zhang, J.; Yin, L.; Hu, G.; Fang, R.; Cheng, H.-M.; Li, F. Conductive porous vanadium nitride/graphene composite as chemical anchor of polysulfides for lithium-sulfur batteries. *Nat. Commun.* **2017**, *8*, 14627.
- (14) Geng, P.; Cao, S.; Guo, X.; Ding, J.; Zhang, S.; Zheng, M.; Pang, H. Polypyrrole coated hollow metal—organic framework composites for lithium—sulfur batteries. *J. Mater. Chem. A* **2019**, *7*, 19465—19470.
- (15) Griebel, J. J.; Nguyen, N. A.; Astashkin, A. V.; Glass, R. S.; Mackay, M. E.; Char, K.; Pyun, J. Preparation of dynamic covalent polymers via inverse vulcanization of elemental sulfur. *ACS Macro Lett.* **2014**, *3*, 1258–1261.
- (16) Zhang, Y.; Glass, R. S.; Char, K.; Pyun, J. Recent advances in the polymerization of elemental sulphur, inverse vulcanization and methods to obtain functional Chalcogenide Hybrid Inorganic/Organic Polymers (CHIPs). *Polym. Chem.* **2019**, *10*, 4078–4105.
- (17) Zhang, T.; Song, Z.; Zhang, J.; Jiang, W.; Mao, R.; Li, B.; Liu, S.; Jian, X.; Hu, F. A semi-immobilized sulfur-rich copolymer backbone with conciliatory polymer skeleton and conductive substrates for high-performance Li-S batteries. *J. Energy Chem.* **2023**, *81*, 510–518.
- (18) Wang, W.; Cao, Z.; Elia, G. A.; Wu, Y.; Wahyudi, W.; Abou-Hamad, E.; Emwas, A.-H. M.; Cavallo, L.; Li, L.-J.; Ming, J. Recognizing the Mechanism of Sulfurized Polyacrylonitrile Cathode Materials for Li–S Batteries and beyond in Al–S Batteries. *ACS Energy Lett.* **2018**, *3*, 2899–2907.
- (19) Xue, W.; Xu, W.; Wang, W.; Gao, G.; Wang, L. Iodine-doped fibrous sulfurized polyacrylonitrile with accelerated reaction kinetics. *Compos. Commun.* **2022**, *30*, 101078.
- (20) Wang, Z.; Shen, X.; Li, S.; Wu, Y.; Yang, T.; Liu, J.; Qian, T.; Yan, C. Low-temperature Li-S batteries enabled by all amorphous conversion process of organosulfur cathode. *J. Energy Chem.* **2022**, *64*, 496–502.

- (21) Cao, Y.; Wu, H.; Li, G.; Liu, C.; Cao, L.; Zhang, Y.; Bao, W.; Wang, H.; Yao, Y.; Liu, S.; et al. Ion selective covalent organic framework enabling enhanced electrochemical performance of lithium—sulfur batteries. *Nano Lett.* **2021**, 21, 2997—3006.
- (22) Shi, J.; Su, M.; Li, H.; Lai, D.; Gao, F.; Lu, Q. Two-Dimensional Imide-Based Covalent Organic Frameworks with Tailored Pore Functionality as Separators for High-Performance Li–S Batteries. ACS Appl. Mater. Interfaces 2022, 14, 42018–42029.
- (23) Wu, Z.; Liang, H.; Lu, J. Synthesis of poly (N-isopropylacrylamide) poly (ethylene glycol) miktoarm star copolymers via RAFT polymerization and aldehyde aminooxy click reaction and their thermoinduced micellization. *Macromolecules* **2010**, *43*, 5699–5705.
- (24) Jiang, Q.; Li, Y.; Zhao, X.; Xiong, P.; Yu, X.; Xu, Y.; Chen, L. Inverse-vulcanization of vinyl functionalized covalent organic frameworks as efficient cathode materials for Li–S batteries. *J. Mater. Chem.* A **2018**, *6*, 17977–17981.
- (25) Hawley, W. B.; Du, Z.; Kukay, A. J.; Dudney, N. J.; Westover, A. S.; Li, J. Deconvoluting sources of failure in lithium metal batteries containing NMC and PEO-based electrolytes. *Electrochim. Acta* **2022**, 404, 139579.
- (26) Kim, D.-W. Electrochemical characterization of poly (ethylene-co-methyl acrylate)-based gel polymer electrolytes for lithium-ion polymer batteries. *J. Power Sources* **2000**, *87*, 78–83.
- (27) Williamson, A. W. XXII.—On etherification. Q. J. Chem. Soc. 1852, 4, 229–239.
- (28) Chen, J.; Franking, R.; Ruther, R. E.; Tan, Y.; He, X.; Hogendoorn, S. R.; Hamers, R. J. Formation of molecular monolayers on TiO2 surfaces: a surface analogue of the Williamson ether synthesis. *Langmuir* **2011**, *27*, 6879–6889.
- (29) Durcik, M.; Toplak, Z. a.; Zidar, N.; Ilaš, J.; Zega, A.; Kikelj, D.; Mašič, L. P.; Tomašič, T. Efficient synthesis of hydroxy-substituted 2-aminobenzo [d] thiazole-6-carboxylic acid derivatives as new building blocks in drug discovery. ACS omega 2020, 5, 8305–8311.
- (30) Wadi, V. S.; Jena, K. K.; Halique, K.; Rožič, B.; Cmok, L.; Tzitzios, V.; Alhassan, S. M. Scalable High Refractive Index polystyrene-sulfur nanocomposites via in situ inverse vulcanization. *Sci. Rep.* **2020**, *10*, 14924.
- (31) Ruffo, R.; Wessells, C.; Huggins, R. A.; Cui, Y. Electrochemical behavior of LiCoO2 as aqueous lithium-ion battery electrodes. *Electrochem. Commun.* **2009**, *11*, 247–249.
- (32) Yang, Y.; Liang, S.; Lu, B.; Zhou, J. Eutectic electrolyte based on N-methylacetamide for highly reversible zinc-iodine battery. *Energy Environ. Sci.* **2022**, *15*, 1192–1200.
- (33) Shi, C.; Shao, S.; Zong, C.; Gu, J.; Huang, Z.; Wang, Q.; Hong, B.; Wang, M.; Zhang, Z.; Li, J.; et al. Thiol for interfacial modification to improve the performance of lithium—sulfur batteries. *Mater. Chem. Front.* **2023**, *7*, 145–152.
- (34) Wang, Z.; Liu, Y.; Ni, J.; You, Y.; Cai, Y.; Zhang, H. Self-Assembled Networks for Regulating Lithium Polysulfides in Lithium-Sulfur Batteries. *ChemSusChem* **2022**, *15*, No. e202201670.
- (35) Tian, J. H.; Jiang, T.; Wang, M.; Hu, Z.; Zhu, X.; Zhang, L.; Qian, T.; Yan, C. In situ/operando spectroscopic characterizations guide the compositional and structural design of lithium—sulfur batteries. *Small Methods* **2020**, *4*, 1900467.
- (36) Cheng, Q.; Chen, Z.-X.; Li, X.-Y.; Hou, L.-P.; Bi, C.-X.; Zhang, X.-Q.; Huang, J.-Q.; Li, B.-Q. Constructing a 700 Wh kg— 1-level rechargeable lithium—sulfur pouch cell. *J. Energy Chem.* **2023**, *76*, 181–186.
- (37) Simmonds, A. G.; Griebel, J. J.; Park, J.; Kim, K. R.; Chung, W. J.; Oleshko, V. P.; Kim, J.; Kim, E. T.; Glass, R. S.; Soles, C. L.; et al. Inverse vulcanization of elemental sulfur to prepare polymeric electrode materials for Li–S batteries. *ACS Macro Lett.* **2014**, *3*, 229–232.
- (38) Yang, L.; Xiong, X.; Liang, G.; Li, X.; Wang, C.; You, W.; Zhao, X.; Liu, X.; Che, R. Atomic Short-Range Order in a Cation-Deficient Perovskite Anode for Fast-Charging and Long-Life Lithium-Ion Batteries. *Adv. Mater.* **2022**, *34*, 2200914.

- (39) Yuan, Y.; Li, Z.; Peng, X.; Xue, K.; Liu, M.; Fang, Z.; Wang, L.; Du, H.; Lu, H. Functional gel cathode strategy to enhance the long-term cyclability of the lithium-polysulfide full cell. *Electrochim. Acta* **2022**, *410*, 140052.
- (40) Dong, Q.; Wei, M.; Zhang, Q.; Xiao, L.; Cai, X.; Zhang, S.; Gao, Q.; Fang, Y.; Peng, F.; Yang, S. Photoassisted Li-ion deintercalation and Ni δ + valence conversion win-win boost energy storage performance in Ni/CdS@ Ni3S2-based Li-ion battery. *Chem. Eng. J.* **2023**, 459, 141542.
- (41) Peng, P.; Wang, Y.; Jiang, F. Numerical study of PCM thermal behavior of a novel PCM-heat pipe combined system for Li-ion battery thermal management. *Appl. Therm. Eng.* **2022**, 209, 118293.
- (42) Sarchami, A.; Najafi, M.; Imam, A.; Houshfar, E. Experimental study of thermal management system for cylindrical Li-ion battery pack based on nanofluid cooling and copper sheath. *Int. J. Therm. Sci.* **2022**, *171*, 107244.
- (43) Gauthier, R.; Luscombe, A.; Bond, T.; Bauer, M.; Johnson, M.; Harlow, J.; Louli, A.; Dahn, J. R. How do depth of discharge, C-rate and calendar age affect capacity retention, impedance growth, the electrodes, and the electrolyte in Li-ion cells? *J. Electrochem. Soc.* **2022**, *169*, 020518.
- (44) Zhang, Q.; Takeuchi, K. J.; Takeuchi, E. S.; Marschilok, A. C. Progress towards high-power Li/CF x batteries: electrode architectures using carbon nanotubes with CF x. *Phys. Chem. Chem. Phys.* **2015**, *17*, 22504–22518.
- (45) Hwang, G.; Sitapure, N.; Moon, J.; Lee, H.; Hwang, S.; Sang-Il Kwon, J. Model predictive control of Lithium-ion batteries: Development of optimal charging profile for reduced intracycle capacity fade using an enhanced single particle model (SPM) with first-principled chemical/mechanical degradation mechanisms. *Chem. Eng. J.* 2022, 435, 134768.

TRecommended by ACS

 $V_2O_5@ZIF\text{-}8$ with a Stable Structure and a Fast Ion Diffusion Channel as a Promising Cathode Material for Lithium-Ion Batteries

Yueming Xin, Daosheng Sun, et al.

JUNE 28, 2023

ACS APPLIED ELECTRONIC MATERIALS

READ 🗹

Cation-Driven Assembly of Bilayered Vanadium Oxide and Graphene Oxide Nanoflakes to Form Two-Dimensional Heterostructure Electrodes for Li-Ion Batteries

Ryan Andris, Ekaterina Pomerantseva, et al.

MAY 22, 2023

ACS APPLIED MATERIALS & INTERFACES

READ 🗹

Interfacial Modification to Nanoflower-Like NiV-Layered Double Hydroxide for Enhancing Supercapacitor Performance

Guorong Wang, Zhiliang Jin, et al.

MAY 10, 2023

ACS APPLIED NANO MATERIALS

READ 🗹

Solvothermal Synthesis of Organic-Inorganic Cathode Vanadyl Acetate Nanobelts for Aqueous Zinc-Ion Batteries

Yunbo Li, Youzhong Dong, et al.

MARCH 22, 2023

ACS SUSTAINABLE CHEMISTRY & ENGINEERING

READ 🗹

Get More Suggestions >